

TEXTS-DIFF: TEXTS-AWARE DIFFUSION MODEL FOR REAL-WORLD TEXT IMAGE SUPER-RESOLUTION

Haodong He*, Xin Zhan*, Yancheng Bai†, Rui Lan, Lei Sun, Xiangxiang Chu

Amap, Alibaba Group

ABSTRACT

Real-world text image super-resolution aims to restore overall visual quality and text legibility in images suffering from diverse degradations and text distortions. However, the scarcity of text image data in existing datasets results in poor performance on text regions. In addition, datasets consisting of isolated text samples limit the quality of background reconstruction. To address these limitations, we construct Real-Texts, a large-scale, high-quality dataset collected from real-world images, which covers diverse scenarios and contains natural text instances in both Chinese and English. Additionally, we propose the TEXTS-Aware Diffusion Model (TEXTS-Diff) to achieve high-quality generation in both background and textual regions. This approach leverages abstract concepts to improve the understanding of textual elements within visual scenes and concrete text regions to enhance textual details. It mitigates distortions and hallucination artifacts commonly observed in text regions, while preserving high-quality visual scene fidelity. Extensive experiments demonstrate that our method achieves state-of-the-art performance across multiple evaluation metrics, exhibiting superior generalization ability and text restoration accuracy in complex scenarios. All the code, model, and dataset will be released.

Index Terms— text image, super-resolution, diffusion model, text-awareness

1. INTRODUCTION

Real-world image super-resolution (Real-ISR) [1] aims to reconstruct high-resolution (HR) contents from low-resolution (LR) images degraded by complex real-world factors. The derived task of real-world text image super-resolution (Real-TISR) encounters an even tougher scenario: it requires not only the reconstruction of global scene details to ensure visual coherence, but also the precise restoration of character structures in text regions. This necessitates that the model needs to simultaneously preserve the super-resolution (SR) quality of both background and text regions.

However, existing SR benchmark datasets [2, 3] contain a relatively small number of images with textual content, and no corresponding text annotations are provided. Although some datasets [4, 5, 6] provide annotated image-text pairs, limitations such as limited scale, isolated text, or monolingual composition constrain their practical applicability. The absence of high-quality text image datasets for this task has limited the generalization of existing models, even though they exhibit remarkable performance in general image [7, 8, 9]. They yield distorted glyphs, missing strokes, or hallucinated characters in the text super-resolution results, primarily due to the



Fig. 1. Example images from other datasets and our Real-Texts dataset. Our dataset includes Chinese and English text across a wide range of scene types and font styles.

minimal attention paid to textual regions. In addition, many dedicated text SR methods [10, 11, 12] enhance only the legibility of cropped text patches while ignoring the surrounding background, leading to significant performance degradation when applied to LR images from complex natural scenes. Consequently, current models struggle to effectively balance textual and background regions, which poses a significant challenge for real-world applications.

To remedy these issues, we construct Real-Texts, a large-scale text image SR dataset. It contains more than 30,000 real-world images with bilingual text (Chinese and English), covering a variety of font styles and diverse scene types. Meanwhile, to achieve high-quality generation in both background and textual regions, we draw inspiration from the global-to-local cognitive pattern in human reading, and propose TEXTS-Diff, a text-aware one-step diffusion model for the Real-TISR task. Specifically, we use the abstract concept of “TEXTS” as a semantic anchor within the primary visual features of LR images, guiding these visual cues to establish text-aware conceptual representations. We then fuse these visual cues with high-level features from the text detection model to further enhance their perception of concrete text regions. Finally, conditioned on the guidance of these visual cues, the diffusion model performs one-step image SR, significantly improving text legibility, while maintaining the ability to super-resolve the entire image and achieve fast inference.

Our contributions are: 1) We construct Real-Texts, a text SR image dataset. It contains more than 30,000 Chinese-English images captured under diverse scenes and font styles. 2) We introduce TEXTS-Diff, which incorporates both abstract text concepts and concrete text regions into visual cues to guide the diffusion process, thereby enhancing the restoration of textual structures in images. 3) Extensive experiments demonstrate that our approach surpasses current methods on dedicated text image SR benchmarks and also delivers competitive performance on general SR datasets.

* Equal contribution

† Project leader: Yancheng Bai

Email: haodonghe@whu.edu.cn, xinzhan@hust.edu.cn, {yancheng.byc, lr264907, ally.sl, chuxiangxiang.cxx}@alibaba-inc.com

Dataset	Text	Bilingual	Font	Scene	#Img	Text line
RealSR [13]	✗	✗	✗	✗	559	-
TextZoom [4]	✓	✗	✗	✗	1,059	21,740
TextOCR [6]	✓	✗	✓	✓	28,134	-
Real-CE [5]	✓	✓	✗	✓	2,718	33,789
Real-Texts	✓	✓	✓	✓	34,875	136,136

Table 1. Comparison between Real-Texts and other datasets.

2. REAL-TEXTS DATASET

Real-TISR task requires a dataset that includes images containing textual content together with their corresponding bounding boxes and text labels. As shown in Table 1, although general SR datasets such as RealSR [13], Flickr2K [2], and LSDIR [3] provide high-quality images, they contain a limited number of images with text and provide no associated annotations. TextZoom [4] annotates existing SR datasets [13, 14], but its scale and diversity are somewhat limited. TextOCR [6] is a large-scale SR dataset (containing 903,069 words). Although it has diverse font styles and scene types, it contains only English text, which limits its linguistic richness. In contrast, Real-CE [5] contains images with both Chinese and English text, but its scale is limited. Recent work [15] synthesizes data by overlaying text onto images. It leads to a noticeable gap from natural images, because the pasted text is unrelated to the background. To address these limitations, we construct the Real-Texts dataset.

2.1. Dataset Creation Process

We collect a set of real-world images with varying resolutions. Then, we apply PPOCRv5 [16] for text detection and recognition, removing any images without valid OCR results. Each retained image (a total of 72,476) is subsequently cropped into regions of 512×512 pixels according to the detected text bounding boxes. In this way, a total of 74,035 cropped images are obtained. These cropped images are then assessed with the VisualQuality-R1 model [17] to obtain quality scores. After automatically filtering the images by a preset threshold of 4.25, we further manually verified the results to ensure high quality. Finally, following the degradation pipeline of Real-ESRGAN [1], we generate the LR counterparts. Through these processes, 34,875 pairs of images are eventually obtained.

2.2. Dataset Analysis

Real-Texts contains 34,875 LR–HR image pairs with both Chinese and English text, covering various scenarios and font styles. As shown in Figure 1, the fonts encompass various styles, including printed, artistic, and calligraphic fonts, while the image scenes feature diverse types such as street views (6,124), posters (5,910), indoor scenes (19,223), and natural scenes (3,618). The dataset contains a total of 136,136 textual instances, including 75,962 Chinese, 37,971 English, and 3,476 mixed Chinese and English instances, while the remaining 18,727 correspond to texts or symbols from other languages. We assign 33,875 image pairs to the training dataset and the remaining 1,000 pairs to the test dataset.

3. METHODOLOGY

3.1. Overview Architecture

Current general diffusion-based SR methods [18, 9, 19, 20] exhibit insufficient text awareness, resulting in poor text legibility. Additionally, most of these methods rely on multi-step generation of HR images, which leads to slow inference. To address these limitations,

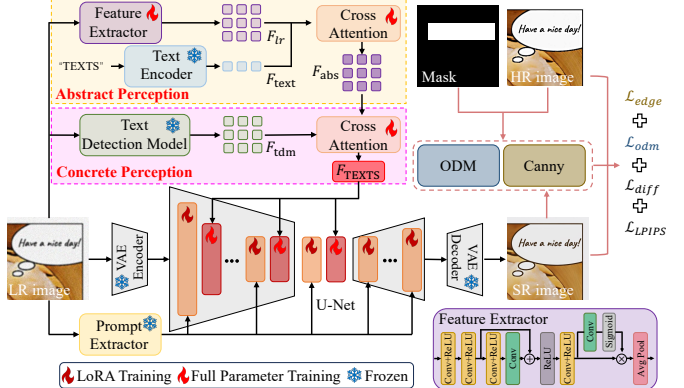


Fig. 2. Overview of TEXTS-Diff. The framework captures text-aware visual cues to guide the diffusion process through abstract and concrete perception processes.

we propose TEXTS-Diff, a one-step diffusion model for Real-TISR. Its overall architecture is illustrated in Figure 2. Inspired by the global-to-local cognitive pattern in human reading, TEXTS-Diff incorporates both abstract text concepts and concrete text regions into visual cues, which are then used as conditions to guide the model’s diffusion process.

3.2. TEXTS-Aware Guidance

Advanced diffusion-based SR models [21, 18] enhance computational efficiency by performing the diffusion process in the latent space of noisy LR images. Nevertheless, the VAE used for latent encoding attenuates high-frequency visual details, which are indispensable for accurate reconstruction of HR images. This loss of information often yields over-smoothed SR outputs, thus degrading the sharpness and continuity of text structures. To address this issue, we propose Feature Extractor ($\mathcal{F}\mathcal{E}$) module (see the bottom-right of Figure 2) to obtain primary visual cues and compensate for information loss. Specifically, $\mathcal{F}\mathcal{E}$ progressively extracts features through stacked convolutional layers and residual blocks. Given an LR image $I_{lr} \in \mathbb{R}^{H \times W \times 3}$, the module produces visual features with high-frequency components better preserved, denoted as F_{lr} :

$$F_{lr} = \mathcal{F}\mathcal{E}(I_{lr}), \quad F_{lr} \in \mathbb{R}^{h \times w \times c}, \quad (1)$$

where $H \times W$ denotes the spatial resolution of the LR image, $h \times w$ refers to the spatial resolution of the LR latent features after 8× downsampling, and c is the channel dimension.

To enable the visual features to form an abstract conceptual understanding of text, we establish a process of textual abstraction perception by applying cross-attention between the visual features F_{lr} and the “TEXTS” textual features F_{text} . The abstract perception process can be expressed as:

$$F_{text} = \mathcal{CLIP}("TEXTS"),$$

$$Q_{lr} = W_q^{lr} \cdot F_{lr}, \quad K_a = W_k^a \cdot F_{text}, \quad V_a = W_v^a \cdot F_{text}, \quad (2)$$

$$F_{abs} = \text{softmax} \left(\frac{Q_{lr} \cdot K_a^T}{\sqrt{d}} \right) \cdot V_a,$$

where \mathcal{CLIP} refers to the text encoder [22], and W_q^{lr} , W_k^a , and W_v^a are learnable linear projection matrices. Q_{lr} , K_a , and V_a denote the query, key, and value matrices, respectively. d indicates the feature dimension, whereas F_{abs} represents the visual feature enhanced by abstract text concepts. In order to enhance the perception of F_{abs} with respect to concrete text regions, we construct a concrete perception

process by applying cross-attention between F_{abs} and the high-level visual features F_{tdm} extracted from the original LR image by the text detection model (\mathcal{TDM}). The process can be defined as:

$$\begin{aligned} F_{\text{tdm}} &= \mathcal{TDM}(I_{lr}), \\ Q_{\text{abs}} &= W_q^{\text{abs}} \cdot F_{\text{abs}}, \quad K_c = W_k^c \cdot F_{\text{tdm}}, \quad V_c = W_v^c \cdot F_{\text{tdm}}, \quad (3) \\ F_{\text{TEXTS}} &= \text{softmax} \left(\frac{Q_{\text{abs}} \cdot K_c^T}{\sqrt{d}} \right) \cdot V_c, \end{aligned}$$

where \mathcal{TDM} denotes DBNet++ [23], and W_q^{abs} , W_k^c , and W_v^c are learnable linear matrices. Q_{abs} , K_c , and V_c denote the query, key, and value matrices, respectively. Through these interaction processes from abstract to concrete, we obtain text-aware enhanced visual features F_{TEXTS} to guide SR.

3.3. Diffusion Processing

We employ a pretrained Stable Diffusion (SD) model as the prior. For practical SR applications, we follow the one-step diffusion technique of OSEDiff [26] by directly transition from the LR image distribution to the HR image distribution in one step. To accommodate this modification, the SD U-Net is fine-tuned using LoRA [27]. To guide the diffusion process, two conditional features are injected into the U-Net: the text-aware feature F_{TEXTS} , and the semantic visual feature F_p extracted from the LR image by a pretrained Prompt Extractor (\mathcal{PE}) [18]. Specifically, F_p is fed into the original Transformer blocks, whereas F_{TEXTS} is supplied to newly added trainable Transformer blocks inserted after each down block and the middle block of the U-Net. Under this guidance, the U-Net refines the latent feature F_v produced by the VAE Encoder and reconstructs the SR image I_{sr} through the VAE Decoder. It can be described as:

$$\begin{aligned} F_v &= \text{Encoder}(I_{lr}), \quad F_p = \mathcal{PE}(I_{lr}), \\ I_{sr} &= \text{Decoder}(\text{U-Net}(F_{\text{TEXTS}}, F_p, F_v)). \quad (4) \end{aligned}$$

3.4. Loss Function

To train our SR framework, we impose an L2-norm loss between the ground truth HR images I_{hr} and the SR predictions I_{sr} to steer the diffusion process. In addition, we incorporate an LPIPS [28] perceptual loss on HR-SR image pairs to encourage the reconstructed images to be perceptually closer to the ground truth. These losses are formulated as follows:

$$\mathcal{L}_{\text{diff}} = \|I_{sr} - I_{hr}\|_2, \quad \mathcal{L}_{\text{LPIPS}} = \text{LPIPS}(I_{sr}, I_{hr}). \quad (5)$$

To enhance text reconstruction in SR images, we use the Canny edge detector to extract edges from SR and HR images, and apply an L2-based edge loss $\mathcal{L}_{\text{edge}}$ for text regions. The OCR-Text Destylization Modeling method (\mathcal{ODM}) [29] is also used to define \mathcal{L}_{odm} , improving the model's sensitivity to textual differences. The losses are formulated as follows:

$$\begin{aligned} \mathcal{L}_{\text{edge}} &= \|(\text{Canny}(I_{sr}) - \text{Canny}(I_{hr})) \circ I_{\text{mask}}\|_2, \\ \mathcal{L}_{\text{odm}} &= \|(\mathcal{ODM}(I_{sr}) - \mathcal{ODM}(I_{hr})) \circ I_{\text{mask}}\|_2, \quad (6) \end{aligned}$$

where \circ denotes the pixel-wise multiplication, and I_{mask} is the binarized ground truth mask based on text line annotations of the HR image. The total loss is formulated as a weighted combination of the above components using λ_1 - λ_4 to balance different aspects of the reconstruction:

$$\mathcal{L}_{\text{total}} = \lambda_1 \mathcal{L}_{\text{diff}} + \lambda_2 \mathcal{L}_{\text{LPIPS}} + \lambda_3 \mathcal{L}_{\text{edge}} + \lambda_4 \mathcal{L}_{\text{odm}}, \quad (7)$$

where λ_1 - λ_4 are set to 1, 2, 1, and 10, respectively.



Fig. 3. Visual comparison on the Real-Texts test dataset. The red box means the poor result areas.

4. EXPERIMENTS

4.1. Experimental Settings

4.1.1. Dataset and Details

The training dataset composition is as follows: 33,875 images with text annotations from the Real-Texts, 14,312 cropped images with text annotations from the Real-CE training set [5], and 20,000 images without text annotations from the LSDIR dataset [3]. We apply the widely used Real-ESRGAN [1] for degradations. We evaluate model performance on the test sets of Real-CE and Real-Texts. For implementation details, we utilize the pretrained SD2.1 model [22] as the backbone. During training, the VAE encoder and decoder are frozen, and the U-Net is fine-tuned via LoRA [27].

4.1.2. Evaluation Metrics

We use OCR accuracy (OCR-A) to evaluate the effectiveness of text SR. Specifically, we evaluate the SR images with text annotations by cropping them based on the ground-truth (GT) text bounding boxes. Subsequently, we compare the text recognition results obtained from the PPOCRV5 [16] with the GT text. To ensure reliability, we manually verify 100 random samples and confirm a text content accuracy of 94.2%. Completely identical text lines are counted as correct, whereas mismatched lines are considered errors. In addition, we use reference-based metrics such as PSNR, SSIM [30], LPIPS [28], DISTS [31], and FID [32], as well as no-reference metrics such as NIQE [33], MANIQA [34], MUSIQ [35], and CLIPQA [36] to evaluate the model's SR performance.

4.2. Experimental Results

4.2.1. Quantitative Comparison

As shown in Table 2, our model achieves state-of-the-art (SOTA) performance on the two annotated datasets (Real-Texts and Real-CE) for text region SR, as measured by OCR-A. Our model's OCR-A surpasses that of the second-best model by 3.67% and 17.60% on Real-Texts and Real-CE, respectively. By comprehensively analyzing both reference-based and non-reference metrics, we achieve the highest total number of best and second-best results on Real-Texts and Real-CE. In addition, the result of RealSR dataset demonstrates that our approach restores text regions without compromising overall image SR quality.

Datasets	Methods	OCR-A \uparrow	PSNR \uparrow	SSIM \uparrow	LPIPS \downarrow	DISTS \downarrow	FID \downarrow	NIQE \downarrow	MANIQA \uparrow	MUSIQ \uparrow	CLIPQA \uparrow
Real-CE	Real-ESRGAN [1]	0.3829	19.10	0.6529	0.3962	0.2460	54.66	5.3908	0.4250	56.56	0.6421
	StableSR [21] (4 steps)	<u>0.3938</u>	19.28	0.6876	0.3472	0.1866	50.04	4.9530	0.4748	49.74	0.5247
	DiffBIR [19] (50 steps)	0.3697	19.96	0.6711	0.3585	0.2251	49.25	5.1390	0.4990	56.29	0.5935
	FaithDiff [20] (20 steps)	0.3691	19.54	0.6569	0.3337	0.1726	42.95	4.1747	0.6189	64.28	0.6619
	SeeSR [18] (50 steps)	0.3846	19.86	0.7078	0.3254	0.2163	48.34	<u>4.6469</u>	0.5770	64.98	0.6884
	SUPiR [24] (50 steps)	0.3590	<u>20.00</u>	0.6584	0.3537	0.1852	44.52	4.6995	0.5344	51.19	0.5525
	OSEDiff [25] (1 step)	0.3758	19.47	0.7097	0.3123	0.1645	49.71	5.2332	0.5933	63.38	0.6439
	TEXTS-Diff (1 step)	0.4631	20.31	0.7235	0.2791	0.1414	<u>44.36</u>	5.4176	0.5590	56.10	0.5439
Real-Texts	Real-ESRGAN [1]	0.3764	22.91	0.7265	0.2794	0.1878	50.12	6.5263	0.5645	67.99	0.6009
	StableSR [21] (4 steps)	0.3511	<u>23.69</u>	<u>0.7481</u>	0.2396	0.1502	36.23	4.8865	0.5867	57.08	0.4707
	DiffBIR [19] (50 steps)	0.3538	22.63	0.6712	0.2709	0.1632	41.76	4.9049	<u>0.6744</u>	72.33	0.6501
	FaithDiff [20] (20 steps)	0.3412	22.82	0.6979	<u>0.2188</u>	<u>0.1448</u>	34.21	4.3931	0.6942	71.43	0.6313
	SeeSR [18] (50 steps)	0.3229	23.09	0.7151	0.2347	0.1750	41.88	5.0474	0.6742	72.69	0.6882
	SUPiR [24] (50 steps)	<u>0.3811</u>	23.23	0.6960	0.2453	0.1454	<u>31.73</u>	4.9894	0.6579	68.94	0.6409
	OSEDiff [25] (1 step)	0.3049	22.91	0.7160	0.2291	0.1476	38.21	4.6753	0.6600	70.12	0.6171
	TEXTS-Diff (1 step)	0.3951	24.49	0.7499	0.1801	0.1174	27.70	<u>4.5296</u>	0.6482	66.18	0.5258
RealSR	Real-ESRGAN [1]	-	25.69	0.7616	0.2727	0.2063	135.18	5.8295	0.5487	60.18	0.4449
	StableSR [21] (4 steps)	-	24.70	0.7085	0.3018	0.2135	128.51	5.9122	0.6221	65.78	0.6178
	DiffBIR [19] (50 steps)	-	24.77	0.6572	0.3658	0.2310	128.99	5.5696	0.6253	64.85	0.6386
	FaithDiff [20] (20 steps)	-	25.32	0.7091	0.2807	<u>0.1922</u>	108.68	4.9688	0.6635	67.37	0.5942
	SeeSR [18] (50 steps)	-	25.18	0.7216	0.3009	0.2223	125.55	5.4081	<u>0.6442</u>	69.77	0.6612
	SUPiR [24] (50 steps)	-	25.16	0.6945	0.3336	0.2102	124.00	<u>5.2011</u>	0.5714	56.94	0.5206
	OSEDiff [25] (1 step)	-	25.15	0.7341	0.2921	0.2128	123.49	5.6476	0.6326	<u>69.09</u>	0.6693
	TEXTS-Diff (1 step)	-	26.51	<u>0.7602</u>	0.2485	0.1842	<u>109.11</u>	5.5610	0.6154	64.82	0.6042

Table 2. Quantitative comparison with state-of-the-art methods on the benchmarks. The best and second-best results of each metric are highlighted in bold and underline, respectively.

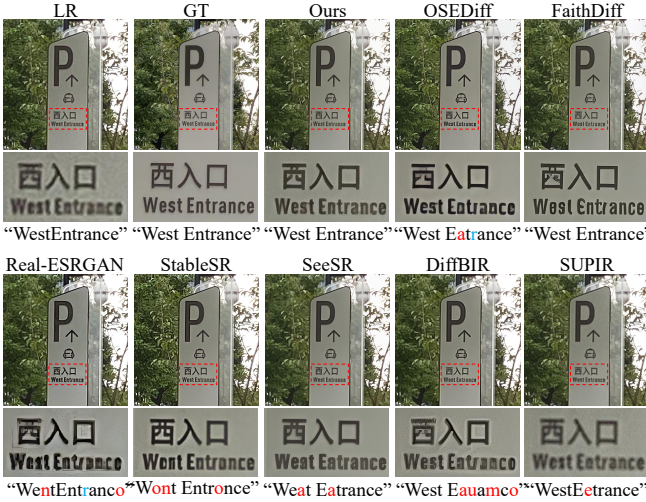


Fig. 4. Visual comparison on the Real-CE validation dataset. The enlarged part of the dashed red box is shown under the original results. Their corresponding OCR recognition results in the aforementioned figure, where erroneous text is highlighted in red and omitted text is marked in blue.

4.2.2. Qualitative Comparison

As shown in the comparison results in Figures 3 and 4, our model consistently outperforms other baseline methods in restoring text regions. Specifically, our SR results significantly improve text legibility for both Chinese and English texts, while avoiding deformation and distortion. Moreover, the model maintains strong performance on non-text regions, effectively preserving overall image quality. These results demonstrate the effectiveness of our model, indicating its potential for practical applications in text image restoration.

Metrics	Ours	w/o TDM	w/o TEXTS	w/o Both
OCR-A \uparrow	0.3951	0.3764	0.3829	0.3715
PSNR \uparrow	<u>24.49</u>	24.46	24.44	24.52
SSIM \uparrow	<u>0.7499</u>	0.7487	0.7480	0.7503
LPIPS \downarrow	0.1801	<u>0.1807</u>	0.1827	0.1826
DISTS \downarrow	0.1174	<u>0.1179</u>	0.1192	0.1180
FID \downarrow	27.70	<u>27.77</u>	28.08	27.88
NIQE \downarrow	<u>4.5296</u>	4.5159	4.6032	4.6619
MANIQA \uparrow	0.6482	<u>0.6514</u>	0.6521	0.6443
MUSIQ \uparrow	66.18	66.71	67.27	66.44
CLIPQA \uparrow	0.5258	<u>0.5358</u>	0.5421	0.5282

Table 3. Ablation study on Real-Texts.

4.2.3. Ablation Study

We conduct experiments on the Real-Texts dataset to evaluate the effectiveness of the “TEXTS” concept and TDM features. The results in Table 3 show that incorporating both abstract and concrete perceptions of text in visual cues can significantly enhance text perception and restoration, while minimally affecting fidelity (PSNR -0.03 dB) and perceptual quality (NIQE +0.0137).

5. CONCLUSION

To address the challenges faced in the real-world text image super-resolution task, we propose Real-Texts, a large-scale, high-quality super-resolution dataset collected from real-world images. In addition, we present TEXTS-Diff, which introduces abstract text concepts and concrete text regions into visual guidance cues and enables one-step generation. This design significantly enhances text super-resolution performance while maintaining its capability to super-resolve image backgrounds.

6. REFERENCES

[1] Xintao Wang, Liangbin Xie, Dong, et al., “Real-esrgan: Training real-world blind super-resolution with pure synthetic data,” in *IEEE ICCV*, 2021, pp. 1905–1914.

[2] Bee Lim, Sanghyun Son, Heewon Kim, et al., “Enhanced deep residual networks for single image super-resolution,” in *IEEE CVPR Workshops*, July 2017.

[3] Yawei Li, Kai Zhang, Liang, et al., “Lsdir: A large scale dataset for image restoration,” in *IEEE CVPR*, 2023, pp. 1775–1787.

[4] Wenjia Wang, Enze Xie, et al., “Scene text image super-resolution in the wild,” in *ECCV*. Springer, 2020, pp. 650–666.

[5] Jianqi Ma, Zhetong Liang, Wangmeng Xiang, et al., “A benchmark for chinese-english scene text image super-resolution,” in *IEEE ICCV*, 2023, pp. 19452–19461.

[6] Amanpreet Singh, Guan Pang, Mandy Toh, et al., “Textocr: Towards large-scale end-to-end reasoning for arbitrary-shaped scene text,” in *IEEE CVPR*, 2021, pp. 8802–8812.

[7] Jianyi Wang, Zongsheng Yue, Shangchen Zhou, et al., “Exploiting diffusion prior for real-world image super-resolution,” *IJCV*, vol. 132, no. 12, pp. 5929–5949, 2024.

[8] Tao Yang, Rongyuan Wu, Peiran Ren, et al., “Pixel-aware stable diffusion for realistic image super-resolution and personalized stylization,” in *ECCV*. Springer, 2024, pp. 74–91.

[9] Fanghua Yu, Jinjin Gu, Zheyuan Li, et al., “Scaling up to excellence: Practicing model scaling for photo-realistic image restoration in the wild,” in *IEEE CVPR*, 2024, pp. 25669–25680.

[10] Jingye Chen, Bin Li, and Xiangyang Xue, “Scene text telescope: Text-focused scene image super-resolution,” in *IEEE CVPR*, 2021, pp. 12026–12035.

[11] Yuzhe Zhang, Jiawei Zhang, Hao Li, et al., “Diffusion-based blind text image super-resolution,” in *IEEE CVPR*, 2024, pp. 25827–25836.

[12] Shipeng Zhu, Zuoyan Zhao, Pengfei Fang, et al., “Improving scene text image super-resolution via dual prior modulation network,” in *AAAI*, 2023, vol. 37, pp. 3843–3851.

[13] Jianrui Cai, Hui Zeng, Hongwei Yong, et al., “Toward real-world single image super-resolution: A new benchmark and a new model,” in *IEEE ICCV*, 2019, pp. 3086–3095.

[14] Xuaner Zhang, Qifeng Chen, Ren Ng, et al., “Zoom to learn, learn to zoom,” in *IEEE CVPR*, 2019, pp. 3762–3770.

[15] Qiming Hu, Linlong Fan, Yiyuan Luo, et al., “Text-aware real-world image super-resolution via diffusion model with joint segmentation decoders,” *arXiv preprint arXiv:2506.04641*, 2025.

[16] Cheng Cui, Ting Sun, Manhui Lin, et al., “Paddleocr 3.0 technical report,” 2025.

[17] Tianhe Wu, Jian Zou, Jie Liang, et al., “Visualquality-r1: Reasoning-induced image quality assessment via reinforcement learning to rank,” *arXiv preprint arXiv:2505.14460*, 2025.

[18] Rongyuan Wu, Tao Yang, Lingchen Sun, et al., “Seesr: Towards semantics-aware real-world image super-resolution,” in *IEEE CVPR*, 2024, pp. 25456–25467.

[19] Xinqi Lin, Jingwen He, Ziyan Chen, et al., “Diffbir: Toward blind image restoration with generative diffusion prior,” in *ECCV*. Springer, 2024, pp. 430–448.

[20] Junyang Chen, Jinshan Pan, and Jiangxin Dong, “Faithdiff: Unleashing diffusion priors for faithful image super-resolution,” in *IEEE CVPR*, 2025, pp. 28188–28197.

[21] Jianyi Wang, Zongsheng Yue, Shangchen Zhou, et al., “Exploiting diffusion prior for real-world image super-resolution,” *IJCV*, vol. 132, no. 12, pp. 5929–5949, 2024.

[22] Robin Rombach, Andreas Blattmann, Dominik Lorenz, et al., “High-resolution image synthesis with latent diffusion models,” in *IEEE CVPR*, 2022, pp. 10684–10695.

[23] Minghui Liao, Zhisheng Zou, Zhaoyi Wan, et al., “Real-time scene text detection with differentiable binarization and adaptive scale fusion,” *IEEE TPAMI*, vol. 45, no. 1, pp. 919–931, 2022.

[24] Fanghua Yu, Jinjin Gu, Zheyuan Li, et al., “Scaling up to excellence: Practicing model scaling for photo-realistic image restoration in the wild,” in *IEEE CVPR*, 2024, pp. 25669–25680.

[25] Rongyuan Wu, Lingchen Sun, Zhiyuan Ma, et al., “One-step effective diffusion network for real-world image super-resolution,” *NeurIPS*, vol. 37, pp. 92529–92553, 2024.

[26] Kangfu Mei, Hossein Talebi, Mojtaba Ardakani, et al., “The power of context: How multimodality improves image super-resolution,” *arXiv preprint arXiv:2503.14503*, 2025.

[27] Edward J Hu, Yelong Shen, Phillip Wallis, et al., “Lora: Low-rank adaptation of large language models,” *arXiv preprint arXiv:2106.09685*, 2021.

[28] Richard Zhang, Phillip Isola, Alexei A Efros, et al., “The unreasonable effectiveness of deep features as a perceptual metric,” in *IEEE CVPR*, 2018, pp. 586–595.

[29] Chen Duan, Pei Fu, Shan Guo, et al., “Odm: A text-image further alignment pre-training approach for scene text detection and spotting,” in *IEEE CVPR*, 2024, pp. 15587–15597.

[30] Zhou Wang, Alan C Bovik, Hamid R Sheikh, et al., “Image quality assessment: from error visibility to structural similarity,” *IEEE TIP*, vol. 13, no. 4, pp. 600–612, 2004.

[31] Keyan Ding, Kede Ma, Shiqi Wang, et al., “Image quality assessment: Unifying structure and texture similarity,” *IEEE TPAMI*, vol. 44, no. 5, pp. 2567–2581, 2020.

[32] Martin Heusel, Hubert Ramsauer, Thomas Unterthiner, et al., “Gans trained by a two time-scale update rule converge to a local nash equilibrium,” *NeurIPS*, vol. 30, 2017.

[33] Lin Zhang, Lei Zhang, and Alan C Bovik, “A feature-enriched completely blind image quality evaluator,” *IEEE TIP*, vol. 24, no. 8, pp. 2579–2591, 2015.

[34] Sidi Yang, Tianhe Wu, Shuwei Shi, et al., “Maniq: Multi-dimension attention network for no-reference image quality assessment,” in *IEEE CVPR*, 2022, pp. 1191–1200.

[35] Junjie Ke, Qifei Wang, Yilin Wang, et al., “Musiq: Multi-scale image quality transformer,” in *IEEE ICCV*, 2021, pp. 5148–5157.

[36] Jianyi Wang, Kelvin CK Chan, and Chen Change Loy, “Exploring clip for assessing the look and feel of images,” in *AAAI*, 2023, vol. 37, pp. 2555–2563.